Characterization and HDS Activity of Mesoporous MoS₂ Catalysts Prepared by *in Situ* Activation of Tetraalkylammonium Thiomolybdates

G. Alonso,*,†,1 G. Berhault,‡ A. Aguilar,* V. Collins,* C. Ornelas,* S. Fuentes,§ and R. R. Chianelli†

*Departamento de Catálisis, Centro de Investigación en Materiales Avanzados, Chihuahua, C.P. 31109, Chih., México; †University of Texas at El Paso, Materials Research Technology Institute, 500 W. University Ave., El Paso, Texas 79968-0685; ‡Laboratoire de Catalyse en Chimie Organique—UMR 6503 CNRS, Université de Poitiers, 40 Avenue du Recteur Pineau, 86022 Poitiers cedex, France; and §Departamento de Catálisis, Centro de Ciencias de la Materia Condensada (CCMC)—UNAM, Apartado postal 2681, 22830, Ensenada, B.C., México

Unsupported molybdenum disulfide catalysts with unique morphological pore structure were synthesized from tetraalkylammonium thiometalates precursors by *in situ* activation during the hydrodesulfurization (HDS) of dibenzothiophene. The precursors used in this study are ammonium thiomolybdate (ATM), tetrapropylammonium thiomolybdate, tetrapentylammonium thiomolybdate, tetrahexylammonium thiomolybdate, tetraheptylammonium thiomolybdate (THepATM), and tetraoctylammonium thiomolybdate. The thermogravimetrical analysis carried out under nitrogen demonstrated that all precursors yield MoS₂ bulk structure at 623 K, after one or two decomposition steps. The morphology of these catalysts observed by scanning electron microscopy presents large hemispherical or ovoid cavities with a cheese-like porous arrangement, high surface area (from 255 up to 329 m²/g), high content of carbon (C/Mo = 2.7–4.0), and type IV adsorption–desorption isotherms of nitrogen. The nature of the alkyl group affects the surface area, the pore size distribution, and the HDS selectivity. The highest selectivity for direct C–S bond cleavage is observed for the molybdenum disulfide catalyst formed from THepATM. X-ray diffraction studies showed that the catalysts are poorly crystallized, with a very weak intensity of the (002) line of 2H-MoS₂ characteristic of exfoliated samples.   © 2002 Elsevier Science (USA)

Key Words: MoS₂; thiosalts; *in situ* activation; mesoporous; hydrodesulfurization.

INTRODUCTION

Transition metal sulfides form a very important group of materials exhibiting a number of interesting properties. One particular chemical property of several of these sulfides is the ability, in the presence of hydrogen, to catalyze sulfur removal from heterocyclic organic molecules such as thiophene, benzothiophene, and dibenzothiophene (1). For this reason, molybdenum disulfide-based solids have been

widely used in the petroleum industry as hydrodesulfurization (HDS) catalysts (1, 2).

Unsupported HDS catalysts have been prepared by different methods, including comaceration (3), homogeneous sulfide precipitation (4), and thiosalt decomposition (5). In these preparation methods, catalysts need to be activated under a H₂/H₂S mixture before being active in catalytic reactions. The catalytic properties of MoS₂ and WS₂ obtained by these methods are reported to depend strongly on the reacting atmosphere, as well as on the heating conditions (3–5). Large variations in surface area have been observed for MoS₂ and WS₂ catalysts, from a few to several tens of square meters per gram, depending on the decomposition conditions (6, 7).

Thiosalt decomposition is an interesting alternative preparation since it provides a simple and reproducible method for obtaining MoS₂ catalysts with controlled stoichiometry. Moreover, these thiosalts have already sulfur bound to the metal atoms in a tetrahedral coordination, and their decomposition has been reported to undergo a topotactic reaction, whereby the *c*-axis of sulfide remains the same as in the precursor (8). Some patents have reported the use of tetraalkylammonium thiometalates to generate carbon-containing MoS₂ and WS₂ catalysts with high surface area and with improved activity (9–12). However, a detailed explanation about their structure and morphology has not been proposed. Such catalysts prepared from tetraalkylammonium thiomolybdates contain certain amounts of carbon and are described with the general formula MoS₂₋ᵧCᵤ, where $0.01 < y < 0.5$ and $0.01 < z < 3.0$ (12). These catalysts exhibit improved activity for the HDS of dibenzothiophene (DBT) (13).

The method of *in situ* decomposition of ammonium thiometalates containing one or two metals (9–11) in a hydrocarbon solution with sulfur organic compounds and pressurized with hydrogen at 623 K yields active metal sulfide. The role of carbon in the formulation of these HDS catalysts is not completely understood, but recent studies

have shown that carbon, at least partly, is included in the arrangement of active sites, probably in the form of surface carbides (14, 15). We have termed these catalysts sulfide-supported carbides to reflect the catalytic stable state (16). Previous studies on catalytic systems based on the *in situ* decomposition of tetraalkylammonium thiotungstates and thiomolybdates have clearly evidenced the formation of sulfur-deficient materials with excess sulfur replaced by carbon at the catalyst surface (14, 17). Moreover, molybdenum carbide catalysts are highly active for hydroprocessing reactions (18–20). Indeed, Sajkowski and Oyama have shown that Mo_2C/Al_2O_3 was three times more active in HDS than MoS_2/Al_2O_3 catalyst (20).

The aim of this work was to obtain MoS_2 catalysts with a unique amorphous morphology from tetraalkylammonium precursors decomposed *in situ* during the HDS of DBT. These as-formed MoS_2-based catalysts were characterized using X-ray diffraction (XRD), energy-dispersive X-ray analysis (EDX), scanning electron microscopy, and nitrogen adsorption at 77 K using the BET isotherm for surface area measurement and the BJH method for pore size distribution. Catalytic activity and selectivity in the HDS of DBT was also reported.

EXPERIMENTAL

Precursor Preparation

The syntheses of the tetraalkylammonium salts $(R_4N)_2MoS_4$ have been reported by McDonald *et al.* (21). In the present work, an improved version of this method was used. The precursors were synthesized at room temperature using an aqueous solution of ammonium tetrathiomolybdate (ATM) $[(NH_4)_2MoS_4]$ and quaternary ammonium halides $[(R_4N)Br$, where $R =$ propyl, pentyl, hexyl, heptyl, and octyl] with yields approximately 80%. The precursor synthesis is reported elsewhere (22). The tetraalkylammonium tetrathiomolybdate salts are referred as TProATM, TPenATM, THexATM, THepATM, and TOctATM when the following respective alkyl groups are used: propyl, pentyl, hexyl, heptyl, and octyl.

Catalytic Activity and Selectivity

The HDS of DBT has been extensively studied as a model reaction of hydrodesulfurization of petroleum feedstock (2). Laboratory-scale studies have been performed in pressurized flow (23) and batch reactors (9–13, 17, 20). By using batch reactors, useful information such as rate constants and selectivity can be obtained by following the composition of the reaction mixture as a function of time. The HDS of DBT was then carried out in a Parr model 4522 high-pressure batch reactor. The appropriate amount of precursor to yield 1 g of MoS_2 catalyst (1.6 g for ATM, 3.73 g for TProATM, 5.11 g for TPenATM, 5.82 g for THexATM, 6.52 g for THepATM, and 7.7 g for TOctATM) was placed in the reactor

with the reagents (5 vol% of DBT in decaline). The catalyst precursors were prepared in tablet form by uniaxial pressing of the thiosalts and were crushed in a mortar before placing them inside the reactor. The reactor was then pressurized to 3.1 MPa with hydrogen and heated to 623 K at a rate of 10 K/min. After the working temperature was reached, sampling for chromatographic analysis was performed during the course of each run to determine conversion versus time dependence. The reaction run time averaged 5 h. The resulting products were analyzed using a Perkin–Elmer Auto-system gas chromatograph with a 6-ft long, 1/8 in. packed column containing OV-3 (phenyl methyl dimethyl silicone, 10% phenyl) as a separating phase.

The main reaction products from the HDS of DBT are biphenyl (BP) and phenylcyclohexane (PCH). Selectivity for the main reaction products (BP, PCH) was determined for MoS_2 catalysts prepared for each precursor and was calculated for a given product as the weight percentage of the product in the product mixture. The mean standard deviation for catalytic measurements was about 2.5%.

Catalyst Characterization

Differential thermal analysis (DTA) and thermogravimetric analysis (TGA) of the thiosalt precursors were made simultaneously on a TA Instrument SDT 2960 DTA–TGA equipment under dry nitrogen flow from 293–1073 K at a heating rate of 10 K/min.

Characterization of catalysts was performed on samples obtained after the catalytic tests. The samples were separated from the reaction mixture by filtration, then washed with isopropanol to remove residual hydrocarbons and dried at room temperature.

A JEOL JSM5800 LV scanning electron microscope was used to perform morphological and elemental analysis. Several fields were analyzed at different magnifications in order to aid in the recognition of the prevalent features.

Specific surface area determination was made with a Quantachrome AUTOSORB-1 model by nitrogen adsorption at 77 K using the BET isotherm. The pore distribution was obtained from the desorption isotherm following the BJH method. Samples were degassed under flowing argon at 473 K for 2 h before nitrogen adsorption. The mean standard deviation for surface area measurements was about 2%.

XRD studies were performed using a Phillips X Pert MPD diffractometer, equipped with a curved graphite monochromator, using $CuK\alpha$ radiation and wavelength λ ($\lambda = 1.54056$ Å) operating at 43 kV and 30 mA.

RESULTS

Thermal Analysis

The data obtained from the DTA–TGA studies of different precursors are summarized in Tables 1–5. DTA
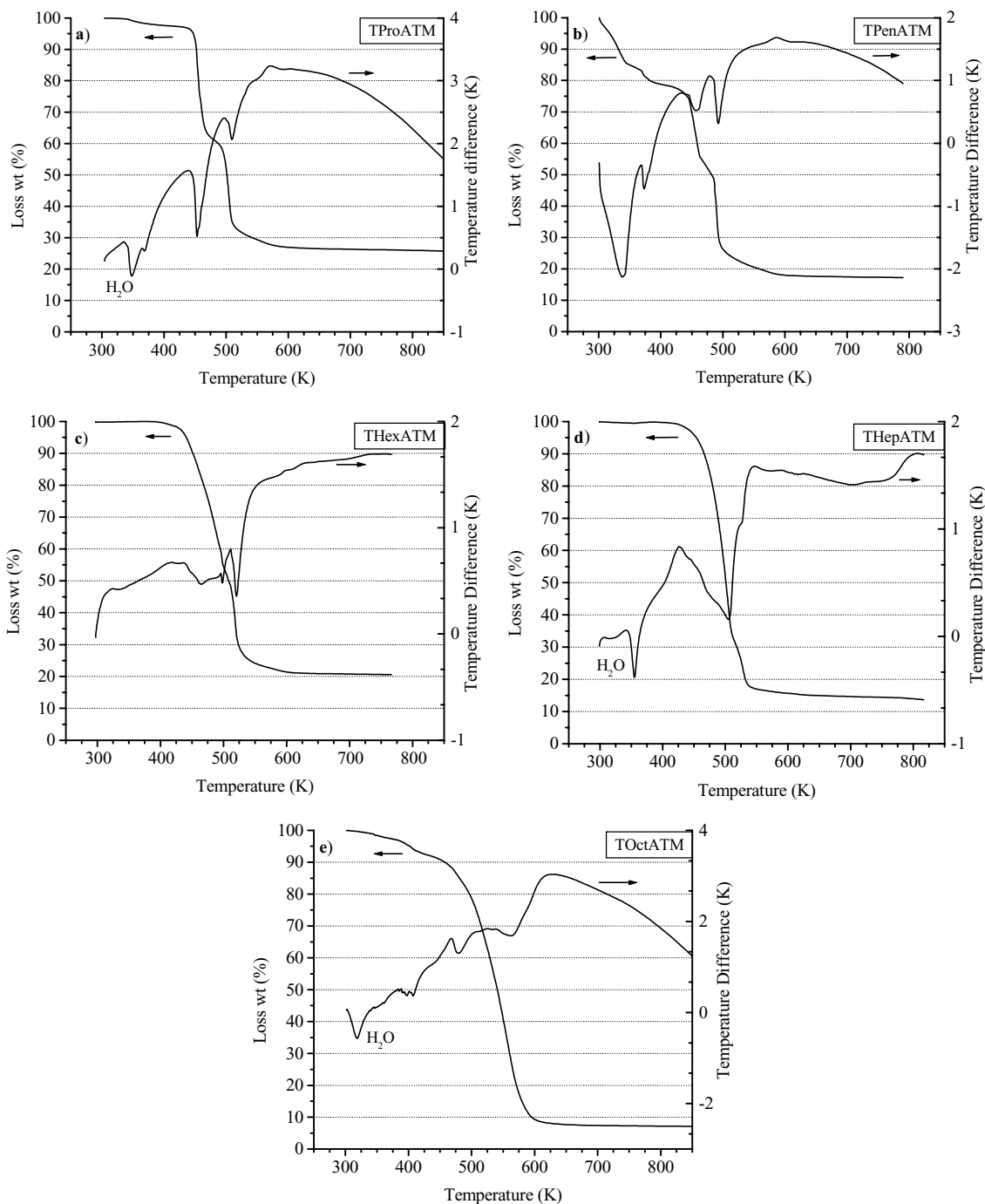
FIG. 1. DTA–TGA curves of the decomposition of the different tetraalkylammonium precursors.

curves corresponding to the decomposition of the catalyst precursors [from TProATM (Fig. 1a) to TOctATM (Fig. 1e)] are reported in Fig. 1. Small weight losses (2% for TProATM, 6% for TOctATM, and less than 1% for THepATM) were observed at low temperatures, around 350 K, with endothermic peaks that may be attributed to the elimination of impurities. Indeed, since these materials were crystallized from a saturated aqueous solution,

some amount of water may be expected to contaminate the thiosalts. Such an early run weight loss has been ascribed to the dehydration of the starting material (24, 25).

Two steps of weight loss are distinguishable from the thermal decomposition of the TProATM and TPenATM precursors with a complicated decomposition pattern involving intramolecular rearrangements and the interaction with neighboring units.
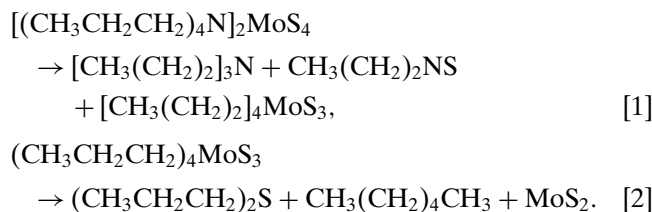
TABLE 1

DTA–TGA Results for the TProATM Precursor Decomposed under Nitrogen Atmosphere

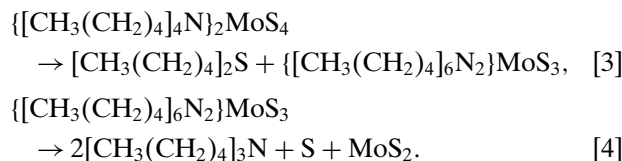| Determinant	TProATM
T_{-1} (K)	360
Δw_{-1}, wt% (exp), assuming water	2.0
T_1 (K)	440
T_2 (K)	493
Δw_1, wt% (exp)	38.0
Δw_1, wt% (theor), assuming loss	38.8
	$[CH_3(CH_2)_2]_3N + CH_3(CH_2)_2N{=}S$
T_3 (K)	623
Δw_2, wt% (exp)	34.0
Δw_2, wt% (theor), assuming loss	34.2
	$[CH_3(CH_2)_2]_2S + CH_3(CH_2)_4CH_3$
$\Sigma\Delta w$, wt% (exp)	72.8
Residual, wt% (exp)	27.2
Residual, wt% (theor), assuming residual as MoS_2	27.0

Note. Δw_{-1} is the experimental weight loss of water observed at temperature T_{-1}, Δw_1, and Δw_2 are experimental and theoretical weight losses of sample during the first step of thermal decomposition at the T_1–T_2 temperature range and during the second step at the T_2–T_3 temperature range, respectively.

According to Table 1, the transitions observed for TProATM are consistent with the following series of reactions:

$$[(CH_3CH_2CH_2)_4N]_2MoS_4$$
$$\rightarrow [CH_3(CH_2)_2]_3N + CH_3(CH_2)_2NS$$
$$+ [CH_3(CH_2)_2]_4MoS_3, \quad [1]$$

$$(CH_3CH_2CH_2)_4MoS_3$$
$$\rightarrow (CH_3CH_2CH_2)_2S + CH_3(CH_2)_4CH_3 + MoS_2. \quad [2]$$

The first step (440–493 K) is proposed to involve elimination of tripropylamine and propylamine sulfide. The second step, at 493–623 K, suggests the elimination of dipropylsulfide and hexane. As shown in Fig. 1a, both steps of decomposition are characterized by an endothermic peak, at 450 and 590 K, respectively.

For TPenATM, the transitions are consistent with reactions [3] and [4] (cf. Table 2):

$$\{[CH_3(CH_2)_4]_4N\}_2MoS_4$$
$$\rightarrow [CH_3(CH_2)_4]_2S + \{[CH_3(CH_2)_4]_6N_2\}MoS_3, \quad [3]$$

$$\{[CH_3(CH_2)_4]_6N_2\}MoS_3$$
$$\rightarrow 2[CH_3(CH_2)_4]_3N + S + MoS_2. \quad [4]$$

Reaction [3] occurs in the 320- to 403-K temperature range and it is proposed to involve elimination of dipentylsulfide. Reaction [4] suggests the elimination of two molecules of tripentylamine plus sulfur from 403 to 623 K. The TGA–
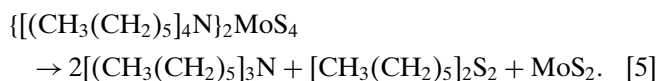
TABLE 2

DTA–TGA Results for the TPenATM Precursor Decomposed under Nitrogen Atmosphere

Determinant	TPenATM
T_1 (K)	320
T_2 (K)	403
Δw_1, wt% (exp)	21.6
Δw_1, wt% (theor), assuming loss	21.3
	$[CH_3(CH_2)_4]_2S$
T_3 (K)	623
Δw_2, wt% (exp)	60.4
Δw_2, wt% (theor), assuming loss	59.5
	$[CH_3(CH_2)_4]_6N_2S$
$\Sigma\Delta w$, wt% (exp)	82.0
Residual, wt% (exp)	18.4
Residual, wt% (theor), assuming residual as MoS_2	19.2

Note. Δw_1 and Δw_2 are experimental and theoretical weight losses of sample during the first step of thermal decomposition at the T_1–T_2 temperature range and during the second step at the T_2–T_3 temperature range, respectively.

DTA analysis in Fig. 1b shows four endothermic peaks during the decomposition reactions. The final product of the thermal decomposition corresponds to nearly stoichiometric MoS_2.

The DTA–TGA results for THexATM and THepATM are reported in Tables 3 and 4, respectively. Contrary to TProATM and TPenATM precursors, the thermal decomposition of THexATM occurs in a single step from 423 to 623 K. It is suggested that during the transition step, two molecules of trihexylamine, and one molecule of dihexyl-disulfide, are directly removed, as shown in the following decomposition reaction:

$$\{[(CH_3(CH_2)_5]_4N\}_2MoS_4$$
$$\rightarrow 2[(CH_3(CH_2)_5]_3N + [CH_3(CH_2)_5]_2S_2 + MoS_2. \quad [5]$$

As shown in Table 4, for THepATM, the transition steps

TABLE 3

DTA–TGA Results for the THexATM Precursor Decomposed under Nitrogen Atmosphere

Determinant	THexATM
T_1 (K)	423
T_2 (K)	623
Δw, wt% (exp)	79.1
Δw, wt% (theor), assuming loss	82.8
	$2[CH_3(CH_2)_5]_3N + [CH_3(CH_2)_5]_2S_2$
Residual, wt% (exp)	20.9
Residual, wt% (theor), assuming residual as MoS_2	17.2

Note. Δw is the experimental and theoretical weight losses of sample during the thermal decomposition at the T_1–T_2 temperature range.

TABLE 4

DTA–TGA Results for the THepATM Precursor Decomposed under Nitrogen Atmosphere

Determinant	THepATM
T_1 (K)	423
T_2 (K)	573
Δw, wt% (exp)	83.0
Δw, wt% (theor), assuming loss	83.2
	$2[CH_3(CH_2)_6]_3N + [CH_3(CH_2)_6]_2S_2$
Residual, wt% (exp)	17.0
Residual, wt% (theor), assuming residual as MoS₂	16.8

Note. Δw is the experimental and theoretical weight losses of sample during the thermal decomposition at the T_1–T_2 temperature range.
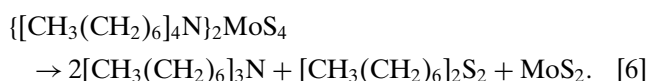
are consistent with the reaction

$$\{[CH_3(CH_2)_6]_4N\}_2MoS_4$$
$$\rightarrow 2[CH_3(CH_2)_6]_3N + [CH_3(CH_2)_6]_2S_2 + MoS_2. \quad [6]$$

This reaction occurs from 423 to 573 K in a single step. Two molecules of triheptylamine and one molecule of diheptyldisulfide are directly removed. In both cases, the hexyl or heptyl groups would react with the S^{2-} ions of the MoS_4^{2-} unit to give disulfide compounds. Figures 1c and 1d report the TGA–DTA analysis of THexATM and THepATM precursors, respectively. In both cases the reactions of decomposition are endothermic. However, the THexATM DTA curve occurring from 400 to 600 K appears more complicated, while for THepATM, a quite important wide peak is observed at 500 K.

Finally, according to Table 5, the thermal decomposition of TOctATM also occurs in a single step from 423 to 623 K with the formation of two molecules of octylamine and one

TABLE 5

DTA–TGA Results for the TOctATM Precursor Decomposed under Nitrogen Atmosphere

Determinant	TOctATM
T_{-1} (K)	383
Δw_{-1}, wt% (exp), assuming water	6.0
T_1 (K)	423
T_2 (K)	623
Δw_1, wt% (exp)	86.5
Δw_1, wt% (theor), assuming loss	86.2
	$2[CH_3(CH_2)_7]_3N + [CH_3(CH_2)_7]_2S_2$
Residual, wt% (exp)	13.5
Residual, wt% (theor), assuming residual as MoS₂	13.8

Note. Δw_{-1} is the experimental weight loss of water observed at temperature T_{-1}. Δw_1 is the experimental and theoretical weight loss of sample during the thermal decomposition at the T_1–T_2 temperature range.

molecule of dioctyldisulfide:

$$\{[CH_3(CH_2)_7]_4N\}_2MoS_4$$
$$\rightarrow 2[(CH_3(CH_2)_7]_3N + [CH_3(CH_2)_7]_2S_2 + MoS_2. \quad [7]$$

Figure 1e shows that the TOctATM DTA curve presents some undefined endothermic peaks during the decomposition reaction occurring from 400 to 630 K. As observed before with the THexATM and THepATM salts, the S^{2-} ions of the MS_4^{2-} unit would react with the octyl groups to give disulfide compounds.

Elemental Analysis

The S/Mo and C/Mo atomic ratios were determined using EDX analysis and are reported in Table 6. A crystalline MoS₂ flake was used for calibration of Mo and S signals. The S/Mo ratio for all catalysts stays constant to a stoichiometric value of 2.0. EDX analysis reveals high C/Mo ratios (2.7–4.5) for the catalysts activated through the *in situ* decomposition of the tetraalkylammonium salts during the HDS of DBT whereas a low C/Mo ratio is found for the ATM-derived catalyst (0.5). Even if the amount of carbon varies strongly with the type of precursor, no clear relationship could be observed between the size of the alkyl group in the thiosalt precursor and the final amount of carbon. However, it appears that C/Mo ratios slightly increase with the number of C atoms initially present in the precursor, with the noticeable exception of TPenATM. Indeed, the MoS₂ catalyst formed from TProATM has a lower C/Mo ratio than the catalyst derived from TOctATM. They have a stoichiometry, respectively, of $MoS_{2.0}C_{3.5}$ and $MoS_{2.0}C_{4.5}$. The TPenATM salt gives rise to a final stoichiometry of $MoS_{2.0}C_{2.7}$. The high amount of residual carbon may be present in the structure as well as on the surface of the catalysts. Moreover, no relationship could be clearly observed when comparing carbon content and surface area.

TABLE 6

Specific Surface Areas, Total Pore Volume, and Elemental Analysis of Mo, S, and C Atomic Ratios for *in Situ* Prepared Molybdenum Sulfide Catalysts

MoS₂ catalysts from	Specific surface area (m²/g)	Total pore volume (cm³/g)	Elemental analysis	
			S/Mo	C/Mo
ATM	60	0.092	1.7	0.5
TProATM	61	0.175	2.0	3.5
TPenATM	329	0.247	2.0	2.7
THexATM	255	0.429	2.0	3.7
THepATM	267	0.472	2.0	4.0
TOctATM	278	0.546	2.0	4.5

Surface Area and Pore Size Distribution

The size of the alkyl group in the precursor compound has an important effect on the surface area and the total pore volume of the MoS_2-based catalysts (cf. Table 6). The total pore volume exhibits a direct correlation with the length of the organic chain of the precursor since the total pore volume increases from 0.092 cm^3/g for ATM to 0.546 cm^3/g for TOctATM. As observed in Fig. 2, with the exception of ATM and TProATM, all the adsorption–desorption curves correspond to type IV isotherms with a desorption step characteristic of mesoporous materials above the relative pressure of 0.3 for TPenATM and 0.4 for THex-, THep-, and TOctATM.

For ATM- and TProATM-made solids, a poorly developed porous system is observed with a surface area of only 60 m^2/g. Type I isotherms can be considered for both samples. Nevertheless, their different isotherm profiles reveal that the higher pore volume of TProATM is due to the presence of very large mesopores while no difference between these solids can be found in the microporous region.

The nitrogen adsorption isotherm for TPenATM shows the highest surface area (329 m^2/g) but a moderate pore volume (0.247 cm^3/g). This indicates that the surface area is mainly due to microporosity since this solid presents the highest nitrogen adsorption values at low relative pressures (P/P_0) corresponding to the filling of both large and small micropores.

Compared to TPenATM, for catalyst based on THex-, THep-, and TOctATM precursors, the specific surface area decreases. However, the BET values hardly change (255–278 m^2/g) whereas the total pore volume increases when increasing the size of the alkyl group from hexyl to octyl. This result suggests that for these solids the main contri-
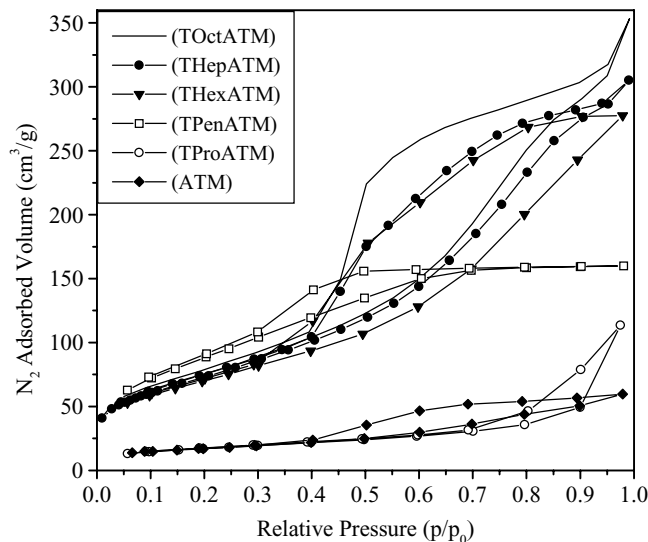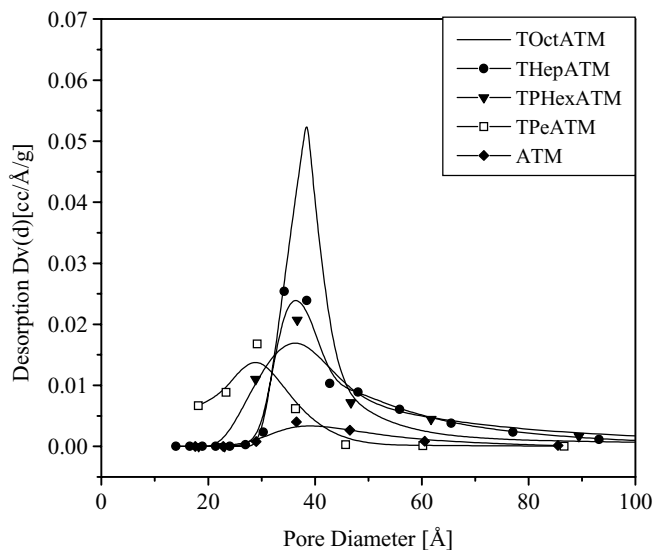

FIG. 3. BJH pore size distribution of MoS_2 catalysts formed by *in situ* decomposition of the different thiometalate precursors.

bution for the development of the pore volume is related to mesopores and that the proportion of micropores versus mesopores probably decreases with increasing alkyl size length. Finally, the hysteresis loops shown by all these catalysts corresponds to cylindrical pores open at both ends.

Figure 3 shows the desorption BJH pore size distribution observed for the MoS_2 catalysts formed from the different thiometalate precursors. Results about TProATM have not been reported since only a very broad pore size distribution is obtained. These catalysts derived from THex-, THep-, and TOctATM precursors present narrow pore size distributions, ranging from 30 to 50 Å, while the mean pore size value for TPenATM shifts downward, to 29 Å. Moreover, its profile suggests a possible bimodal porous distribution with another maximum in the microporous region.

Scanning Electron Microscopy

Images of the final MoS_2 catalysts prepared from (a) TProATM, (b) TPenATM, (c) THexATM, (d) THepATM, and (e) TOctATM are reported Fig. 4. These solids appear very porous, with bubblelike cavities probably resulting from the elimination of gas products. Cavity size seems to increase from TProATM to TPenATM and THexATM while for larger-size alkyl groups, the cavities present slightly smaller diameters. For the THex-, THep-, and TOctATM-made solids, walls between cavities appear thicker than for catalysts made from TPenATM.

X-Ray Diffraction

Figure 5 shows the XRD patterns of the final MoS_2 catalysts prepared from tetraalkylammonium thiometalate precursors. All these patterns are in agreement with those reported for the poorly crystalline MoS_2 structure (24).
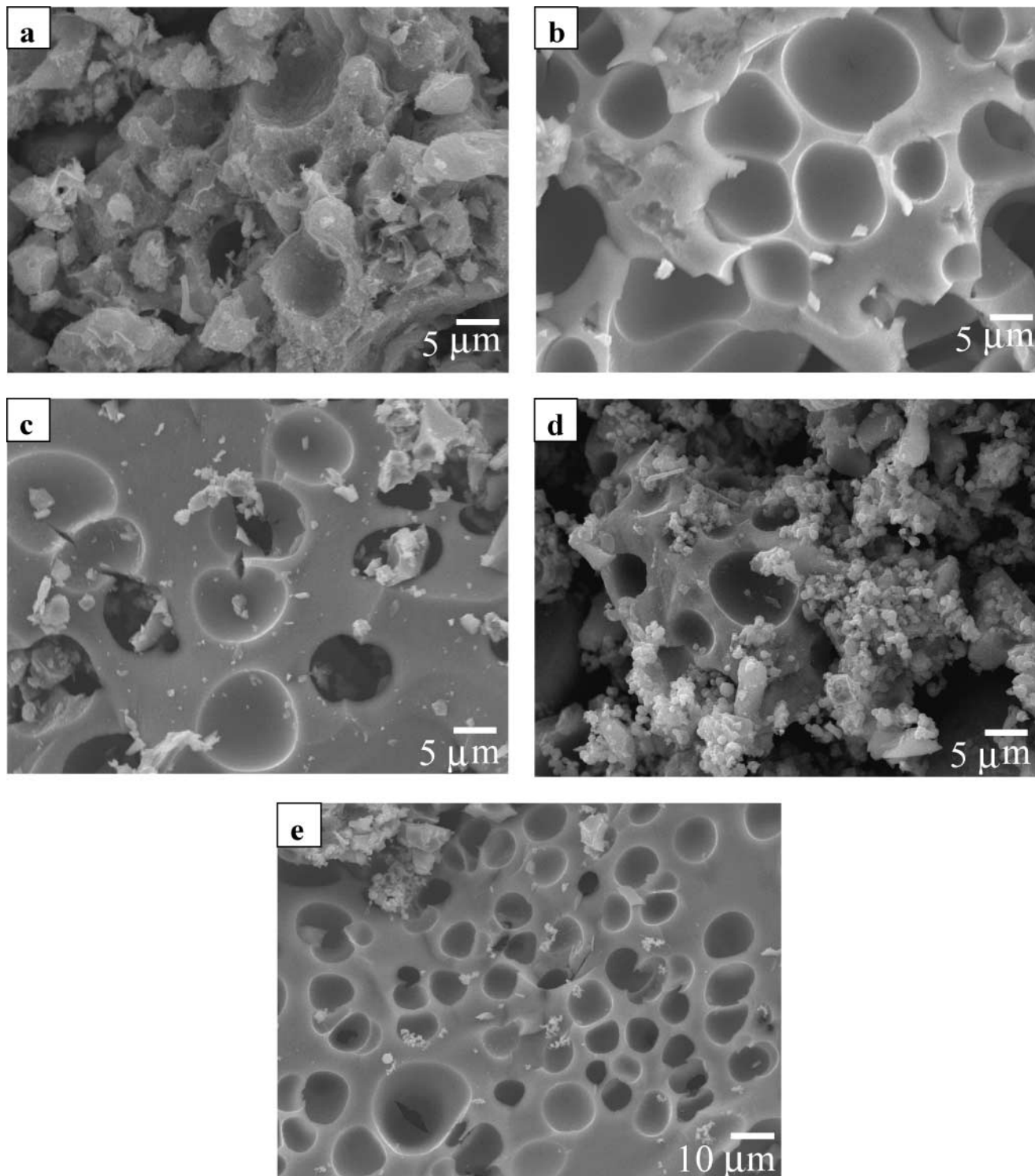

FIG. 2. Adsorption–desorption isotherms for MoS_2 catalysts formed by *in situ* decomposition of the different thiometalate precursors.

FIG. 4. Scanning electron micrographs of the MoS$_2$ catalysts prepared from (a) TProATM, (b) TPenATM, (c) THexATM, (d) HepATM, and (e) TOctATM.

However, for catalysts obtained from ATM and TProATM precursors, a quite strong (002) diffraction peak at $2\Theta = 14°$ can be observed, while for the series from TPenATM- to TOctATM-made catalysts, the (002) peak is very weak. Ac-cordingly, the c-direction layer stacking in the ATM and TProATM-derived catalysts is then higher than for the cata-lysts made from TPenATM, THexATM, THepATM, and TOctATM precursors.
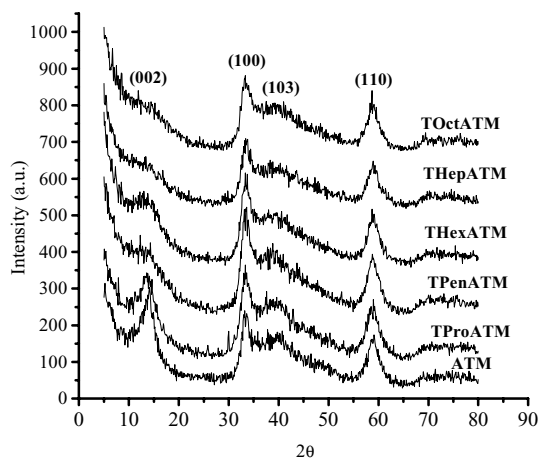
FIG. 5. XRD patterns of MoS$_2$ catalysts formed by *in situ* decomposition of the different thiometalate precursors.

Catalytic Activity and Selectivity

The HDS of DBT yields two main products: biphenyl (BP) through the so-called direct desulfurization pathway (DDS), and phenylcyclohexane (PCH) through the hydrogenative pathway (HYD). Since these two pathways are parallel (26), the ratio between HYD and DDS can be approximated in terms of the experimental selectivity by means of the equation

$$HYD/DDS = (PCH)/(BP).$$

Table 7 summarizes the selectivity for BP and PCH through HYD/DDS ratios measured for different MoS$_2$ catalysts formed by the *in situ* decomposition of tetraalkylammonium thiometalate precursors. Contrary to *ex situ* experiments, for which thiosalt precursors are decomposed before being used for HDS reactions, *in situ* experiments do not reveal significant changes in activity between the ATM precursor and other carbon-containing ATM precursors. ATM, TProATM, and TPenATM precursors lead to similar se-

TABLE 7

Initial Rate Constants, Selectivity (HYD/DDS Ratio), and [THDBT]/[PCH] Ratio of MoS$_2$ Catalysts Prepared by *in Situ* Decomposition of Tetraalkylammonium Precursors during the HDS Reaction of DBT

MoS$_2$ catalysts from	k (specific) ($\times 10^{-7}$, mol · g^{-1} · s^{-1})	HYD/DDS ratio	[THDBT]/[PCH] ratio
ATM	5.9	1.5	1.0
TProATM	5.0	1.5	1.2
TPenATM	5.7	1.7	1.7
THexATM	5.2	0.5	0.4
THepATM	4.4	0.3	0.2
TOctATM	5.4	0.6	0.3

Note. $T = 623$ K, $P = 3.1$ MPa.

lectivity results, with a HYD/DDS ratio of 1.5–1.7. Interestingly, from THexATM to TOctATM, a strong change in selectivity is observed, with lower HYD/DDS values (0.3–0.6). The MoS$_2$ catalyst prepared from THepATM presents the highest selectivity for the direct desulfurization pathway. Hydrogenation of dibenzothiophene to form tetrahydrodibenzothiophene (THDBT) strongly decreases between the series of ATM-, TProATM-, and TPenATM-made catalysts and catalytic systems based on the decomposition of THex-, THep-, and TOctATM precursors.

DISCUSSION

Tetraalkylammonium thiometalate precursors were used *in situ* to prepare MoS$_2$-based catalysts during the HDS reaction. The *in situ* preparation of active sulfide catalysts leads to very high surface area solids (from 60 to 329 m^2/g) with narrow pore size distribution. After the HDS reaction, all these catalysts present large amounts of excess carbon. However, the activity variations are not really marked compared to results reported for *ex situ* methods of preparation (27). *Ex situ* decomposition of precursors (before HDS test) lead to catalytic systems with a very low surface area, in contrast to *in situ* decomposition, and to a final carbon content directly proportional to the size of the precursor's alkyl group. Variations of activity would then be expected to depend on the carbon content of the *ex situ* decomposed catalyst. Anyway, for *in situ* experiments, no clear relationship could be observed between surface area, alkyl size length, and catalytic activity. A slight increase in surface area could be observed when varying the organic chain from propyl to hexyl groups. These results show that even if more active sites could be expected from an increase in surface area, activity change could not be really detected. This situation is common for anisotropic layered materials like MoS$_2$ and this represents a major ongoing characterization challenge in this field.

One may propose that the excess carbon formed during the HDS reaction could play a negative role in the activity by reducing the number of accessible sites. However, the stoichiometry of the catalyst prepared from ATM (MoS$_{1.7}$C$_{0.5}$) is similar to the value expected for stabilized active phases during the course of an HDS run, as reported recently by Berhault *et al.* (15). Indeed, it was observed that starting initially from a MoS$_{2+X}$ stoichiometry, the active phase of a sulfide catalyst progressively accommodates structural carbon by replacing surface sulfur atoms at the edges of MoS$_{2+X}$ layers. This replacement occurs in typical hydrotreating conditions, leading to a final stoichiometry of MoS$_Y$C$_Z$, with $y + z = 2 + x$. Sulfur replacement by structural carbon should be viewed as a process limited to the edges of the layers. Bulk sulfur atoms inside the slabs are not easily replaced by carbon. In fact, using Auger spectroscopy, previous studies (14, 17) about the *in situ* decomposition

of tetraalkylammonium thiometalate salts have confirmed that in the catalytic system studied here, sulfur atoms are replaced by carbon, leading to stabilized sulfur-deficient carbon-containing $MeS_Y C_Z$ catalysts. Then, one may suggest that in the present catalytic systems, a certain amount of structural carbon is included in the stabilized active phase. Nevertheless, after the replacement of all the surface sulfur atoms available, no more carbon replacement should occur since the MoS_2 bulk structure would stay sulfidic by nature. In this case, the carbon excess would be formed by blocking active sites. Consequently, the beneficial effect of structural carbon would be counterbalanced by the formation of carbon in excess, resulting in the absence of improved HDS activity.

More interestingly, while there is no change in selectivity for catalysts prepared from TProATM and TPenATM compared to ATM, strong change is observed for catalysts prepared by *in situ* decomposition of THex-, THep-, and TOctATM precursors. These catalysts present characteristic type IV isotherms while TProATM-made catalysts do not present a type IV isotherm and TPenATM presents only a small hysteresis. This could be related to the different decomposition modes between TProATM and TPenATM, with two steps of decomposition, and THex-, THep-, and TOctATM, with only a single step. Moreover, according to XRD results, THex-, THep-, and TOctATM-made catalysts demonstrate large morphological modifications compared to ATM and TProATM-made catalysts. Indeed, their layered structure is largely less stacked than for catalysts derived from ATM and TProATM precursors. The rim–edge model was previously developed by Daage and Chianelli (28) in order to explain selectivity changes for the HDS of dibenzothiophene using geometrical considerations. Since the MoS_2 particles are composed of stacked layers, different types of active sites could be found. While extremities of the stacked layers possess active sites (called rim sites) for both hydrogenation and HDS reactions, other active sites located on "internal" stacked layers (called edge sites) are only active for HDS reactions. It should be underlined that the terminology used here could differ from previous studies. Indeed, Massoth *et al.* (29) and Topsøe *et al.* (30) have envisaged that corner sites would be responsible for HDS reactions while hydrogenation occurs on edge sites (equivalent in that case to both edge and rim sites, according to the rim–edge model). However, these results were obtained for the gas-phase HDS of thiophene whereas the rim–edge model, as in our study, was based on liquid-phase DBT HDS results. A recent study by Hensen *et al.* (31) has demonstrated that considerations based on the rim–edge model should not be used to explain selectivity changes in the HDS of thiophene. Moreover, "corner–edge" models were based on the assumption that each layer is chemically independent of each other since interlayer forces are only due to van der Waals interactions. These models then

predict that selectivity will change with particle size along the basal plane. Large molecules like DBT will make inappropriate the assumptions that each layer is chemically independent since, in such cases, steric hindrances during adsorption with neighboring molybdenum atoms in the next layer have to be expected. Finally, even if the particle size along the basal plane cannot be measured using X-ray diffraction, the crystalline order along the basal plane could be estimated using the widening of the (110) peak, as shown Fig. 5. It could then be observed that the crystalline order along this plane is hardly changed for all precursor-made catalysts. This would mean that the fraction of corner sites to edge sites is relatively constant and that according to the corner–edge model, selectivity would not be modified when increasing the alkyl chain length of the precursor, which it does not. Anyway, according to the rim–edge model, steric constraints will hinder the initial η^6-adsorption of the aromatic rings, prerequisite for their hydrogenation. A low HYD/DDS ratio would then be expected for MoS_2 catalysts derived from ATM and TProATM precursors, while in the same spirit, the less stacked morphology of MoS_2 catalysts formed from THex-, THep-, and TOctATM would lead to more hydrogenating catalytic properties. In fact, a reverse effect is observed to what could be predicted based on the rim–edge model. This result leads to the consideration that a simple morphological effect modifying only the relative proportion of rim sites versus edge sites is not sufficient to explain the strong change in selectivity observed in this study. Consequently, the nature itself of the sites is probably altered during the *in situ* process of formation of MoS_2 catalysts derived from THex-, THep-, and TOctATM precursors. This result might be explained through the formation of a "sulfocarbide" phase, as already reported by different authors (13–15, 32–34). Indeed, it was proposed that in typical hydrotreating conditions carbide and sulfide catalysts would tend to a common active surface presenting both S and C moieties (32) and with a more favored selectivity along the direct desulfurization pathway, leading to biphenyl. This mixed carbosulfide phase was also observed in recent studies by Schwartz *et al.* (32) and by Hsu *et al.* (35). However, in this case, the formation of a sulfocarbide phase would be expected for any *in situ* catalyst (derived from both ATM and tetraalkyl–ATM precursors) prepared during the course of the HDS of DBT. Therefore, this would not explain the marked difference in selectivity observed between the series of catalysts made from ATM, TProATM, and TPenATM and those made from THexATM, THepATM, and TOctATM. TGA–DTA results have shown that the decomposition mode of the two series of precursors differs strongly. This may explain the mesoporosity of the second series of catalysts in contrast to catalysts made from ATM and TProATM, for which a similar porous structure was not observed, the TPenATM-made catalyst being an intermediate case. As observed in Fig. 3 and Table 7, the

formation of mesopores is clearly accompanied by a strong change in selectivity for the HDS of DBT. Indeed, the comparison of catalysts made from TPenATM and THexATM shows that change in pore size corresponds to a strong modification in the selectivity, and the HYD/DDS ratio moves from 1.7 to 0.5. The pore size optimum does not change for THex-, THep-, or TOctATM-made catalysts and the selectivity is similar between these three solids. A relationship between mesoporous structure and DDS-selective catalytic systems is evidenced.

It is now well admitted that the prerequisite for hydrogenation is a π-complexation through the aromatic ring. This flatwise mode of adsorption covers a large part of the catalyst surface. Only rim sites present the suitable geometry for adsorbing reactants through the aromatic ring whereas the C–S bond-breaking mechanism first needs a σ bond between the metal center and the sulfur atom. These different modes of adsorption led Daage and Chianelli (28) to consider that hydrogenation of DBT is a steric demanding reaction. This steric requirement does not seem to be achieved in the mesoporous cavities of our catalytic systems, leading to a confinement effect restricting adsorption of reactants on rim sites and change in selectivity. The steric hindrance for hydrogenation could be directly determined when considering the ratio between tetrahydrodibenzothiophene (THDBT), the primary product formed by hydrogenation of one of the aromatic rings along the HYD pathway, and biphenyl (BP), the primary product formed by C–S bond hydrogenolysis along the DDS pathway. For instance, this ratio was used for the rim–edge model to show a direct linear relationship between stacking of the layers and variation in the hydrogenation/hydrogenolysis functions for the HDS of DBT. In the present study, in which stacking is not the main parameter involved in the change in selectivity, formation of mesopores for THex-, THep-, and TOctATM-made catalysts is accompanied by a strong decrease in the [THDBT]/[BP] ratio, from 1.70 for the TPenATM-made catalyst to 0.35 for the THexATM-made one (cf. Table 7). The steric demanding adsorption preceding hydrogenation of DBT seems hindered by confinement inside mesopores and is then responsible for the less hydrogenating properties of these solids. However, in this case, apart from the hypothesis of excess carbon blocking active sites, the apparent absence of activity variation appears surprising since, first, hydrogenation sites would be less accessible for DBT and, second, the number of edge sites would be smaller since the stacking is decreasing when mesoporosity is formed. A total decrease in activity would then be expected, in contrast to experimental results. To solve this contradiction, an increase in the intrinsic activity of the edge sites has to be envisaged. This would be the result of a better "HDS beneficial" interaction of the active phase with the as-formed alkyl disulfides during the *in situ* decomposition of the THexATM, THepATM, and TOctATM precursors. In fact, alkyl disulfides are well-known to be highly efficient presulfiding agents leading to HDS-enhanced active phases (36). It should be underlined that a similar DDS-favored selectivity change effect was recently observed using CoMo catalysts supported on mesoporous Si–MCM-41 (37).

If mesoporosity has mainly been previously observed in oxide-type solids such as alumina, silica, and pillared clays, it has also been recently observed in sulfide materials (38, 39). The cause for a type IV isotherm in some solids has been extensively studied by Everett, who gave possible explanations to the existence of large and wide hysteresis loops (40). One case deserving great attention for amorphous materials is the study by Mayagoitia *et al.* (41, 42), which correlates type IV hysteresis loops with the presence of an extensively interconnected porous network of mesoporous cavities and connecting channels. In MoS_2 catalysts derived from tetraalkylammonium thiometalates, mesoporous cavities are formed because of the accumulation of gases during the precursor decomposition while channels are created during the escape of such gases to the exterior. Such a porous network in amorphous materials may be considered equivalent to the porous structure of molecular sieves, which very likely induce confinement effects. Due to such properties, the high-surface-area MoS_2 materials reported in this work are also called "amorphous mesoporous sulfides."

CONCLUSIONS

MoS_2-based catalysts were prepared by *in situ* decomposition of different tetraalkylammonium thiometalate precursors (with alkyl = propyl, pentyl, hexyl, heptyl, and octyl). The solids obtained using this procedure present interesting morphological properties with high surface area, characteristic type IV isotherms, narrow pore size distribution, and a very dispersed active phase with low-stacked layers. Moreover, for catalysts derived from tetrahexyl-, tetraheptyl-, and tetraoctylammonium precursors, high selectivity along the direct desulfurization pathway was observed while activity was preserved, as compared to ATM-derived MoS_2 catalysts. Results suggest a possible confining effect modifying the HDS selectivity for the mesoporous catalysts formed when decomposing thiometalate precursors with long alkyl groups. This new type of sulfide materials could be named "amorphous mesoporous sulfide" catalysts.

REFERENCES

1. Weisser, O., and Landa, S., "Sulfide Catalysts: Their Properties and Applications." Pergamon Press, New York, 1973.
2. Topsøe, H., Clausen, B. S., and Massoth, F. E., *in* "Hydrotreating Catalysis—Catalysis, Science and Technology" (J. R. Anderson and M. Boudart, Eds.), Vol. 11. Springer-Verlag, Berlin, 1996.
3. Hagenbach, G., Courty, Ph., and Delmon, B., *J. Catal.* **31**, 264 (1973).
4. Candia, R., Clausen, B. S., and Topsøe, H., *J. Catal.* **77**, 564 (1982).
5. Zdrazil, M., *Catal. Today* **3**, 269 (1988).
6. Frety, R., Breysse, M., Lacroix, M., and Vrinat, M., *Bull. Soc. Chim. Belg.* **93**, 663 (1984).
7. Ramanathan, K., and Weller, S., *J. Catal.* **95**, 249 (1985).
8. Frommell, E., Diehl, J., Tamilia, J., and Pollack, S., *in* "Proceedings of the 12th North American Catalysis Society Meeting" (B. H. Davis, Ed.), Lexington, KY, 1991, PD-38.
9. Jacobson, A. J., Chianelli, R. R., and Pecoraro, T. A., U.S. Patent 4,650,563 (1987).
10. Naumann, A. W., and Behan, A. S., U.S. Patent 4,243,554 (1981).
11. Chianelli, R. R., and Pecoraro, T. A., U.S. Patent 4,508,847 (1985).
12. Pecoraro, T. A., and Chianelli, R. R., U.S. Patent 4,528,089 (1985).
13. Alonso, G., Del Valle, M., Cruz-Reyes, J., Licea-Claverie, A., Petranovskii, V., and Fuentes, S., *Catal. Lett.* **52**, 55 (1998).
14. Alonso, G., Petranovskii, V., Del Valle, M., Cruz-Reyes, J., Licea-Claverie, A., and Fuentes, S., *Appl. Catal. A* **197**, 87 (2000).
15. Berhault, G., Mehta, A., Pavel, A. C., Yang, J., Rendon, L., Yácaman, M. J., Cota, L., Duarte, A., and Chianelli, R. R., *J. Catal.* **198**, 9 (2001), doi:10.1006/jcat.2000.3124.
16. Berhault, G., Cota, L., Duarte, A., Mehta, A., and Chianelli, R. R., *Catal. Lett.* **78**, 81 (2002).
17. Alonso, G., Del Valle, M., Cruz-Reyes, J., Licea-Claverie, A., Petranovskii, V., and Fuentes, S., *Catal. Today* **43**, 117 (1998).
18. Lee, J. S., and Boudart, M., *Appl. Catal.* **19**, 207 (1985).
19. Markel, E. J., and van Zee, J. W., *J. Catal.* **126**, 643 (1990).
20. Sajkowski, D. J., and Oyama, S. T., *Appl. Catal. A* **134**, 339 (1996).
21. McDonald, W. J. W., Delbert Friesen, G., Rosehein, L. D., and Newton, W. E., *Inorg. Chim. Acta* **72**, 205 (1983).
22. Alonso, G., Berhault, G., and Chianelli, R. R., *Inorg. Chim. Acta* **316**, 105 (2001).
23. Ishihara, H., Itoh, T., Hino, T., Nomura, M., Qi, P., and Kabe, T., *J. Catal.* **140**, 184 (1993), doi:10.1006/jcat.1993.1077.
24. Wang, H. W., Skeldon, P., Thompson, G. E., and Wood, G. C., *J. Mater. Sci.* **32**, 497 (1997).
25. Hibble, S. J., and Feaviour, M. R., *J. Mater. Chem.* **11**, 2607 (2001).
26. Whitehurst, D. D., Isoda, T., and Mochida, I., *Adv. Catal.* **42**, 345 (1998).
27. Alonso, G., Del Valle, M., Cruz-Reyes, J., and Fuentes, S., *in* "Surfaces, Vacuum and their Applications," Am. Inst. Phys. Conference Proceedings (I. Hernandez-Calderon and R. Asomoza, Eds.), Vol. 378, p. 552. Springer-Verlag, New York, 1996.
28. Daage, M., and Chianelli, R. R., *J. Catal.* **149**, 414 (1994), doi:10.1006/jcat.1994.1308.
29. Massoth, F. E., Muralidhar, G., and Shabtai, J., *J. Catal.* **85**, 53 (1984).
30. Topsøe, H., Candia, R., Topsøe, N.-Y., and Clausen, B. S., *Bull. Soc. Chim. Belg.* **93**, 783 (1984).
31. Hensen, E. J. M., Kooyman, P. J., van der Meer, Y., van der Kraan, A. M., de Beer, V. H. J., van Veen, J. A. R., and van Santen, R. A., *J. Catal.* **199**, 224 (2001), doi:10.1006/jcat.2000.3158.
32. Schwartz, V., Teixeira da Silva, V., and Oyama, S. T., *J. Mol. Chem. A* **163**, 251 (2000).
33. Dhandapani, B., St Clair, T., and Oyama, S. T., *Appl. Catal. A* **168**, 219 (1998).
34. Rodriguez, J. A., Dvorak, J., and Jirsak, T., *J. Phys. Chem. B* **104**, 11515 (2000).
35. Hsu, W. K., Zhu, Y. Q., Firth, S., Terrones, M., Terrones, H., Trasobares, H., Clark, R. J. H., Kroto, H. W., and Walton, D. R. M., *Carbon* **39**, 1107 (2001).
36. Hallie, H., *Oil Gas J.* **48**, 69 (1982).
37. Wang, A., Wang, Y., Kabe, T., Chen, Y., Ishihara, A., and Qian, W., *J. Catal.* **199**, 19 (2001), doi:10.1006/jcat.2000.3148.
38. Rueda, N., Bacaud, R., and Vrinat, M., *J. Catal.* **169**, 404 (1997), doi:10.1006/jcat.1997.1669.
39. Araki, Y., Ywata, Y., Miki, Y., Honna, K., Matsubayashi, N., and Shimada, H., *in* "Hydrotreatment and Hydrocracking of Oil Fractions" (B. Delmon, G. F. Froment, and P. Grange, Eds.), p. 69. Elsevier Science, Amsterdam, 1999.
40. Everett, D. H., *in* "The Solid–Gas Interface" (E. A. Flood, Ed.), Vol. 2, p. 1055. Dekker, New York, 1967.
41. Mayagoitia, V., Rojas, F., and Kornhauser, I., *J. Chem Soc. Faraday Trans. I* **84**, 785 (1988).
42. Mayagoitia, V., Gilot, B., Rojas, F., and Kornhauser, I., *J. Chem Soc. Faraday Trans. I* **84**, 801 (1988).